Annals of Agricultural Science, Moshtohor (ASSJM)
https://assjm.journals.ekb.eg/
www.fagr.bu.edu.eg
© 2023, Faculty of Agriculture, Benha University, Egypt. ISSN:1110-0419
Original Article Vol. 61(4) (2023), 771 –780 DOI:10.21608/assjm.2024.250353.1255

Characterization of Chemically Synthesized Nano-zerovalent-Iron (nZVI) Prepared for Removing Contaminants from Wastewater

E.A. Shehab[2], H.M. Salem[1], S.M. Soliman[2], Y.G.M. Galal[2] and M.A. Abdel-Salam[1]

[1]Soil and water, Faculty of Agriculture, Benha University.
[2] Nuclear Research Center Soil and Water Research Department, Egyptian Atomic Energy Authority, Abou-Zaabal, 13759, Egypt.

Abstract

Water pollution is a global issue, prompting increased efforts to eliminate pollutants from water sources. This study focuses on the preparation and characterization of chemically synthesized nanomaterials, specifically nano-zero-valent iron (nZVI), to be used as absorbents targeting Cd and Pb pollutants. nZVI analysis confirms the presence of predicted components in both irradiated and non-irradiated adsorbent materials. The created nZVI exhibits a 3D square crystallite structure with a crystallite size of 60.80 nm, as revealed by energy dispersive X-ray-equipped scanning electron microscope SEM-EDX. FTIR analysis attributes the significant absorption of Pb and Cd to the O-H stretch functional group vibrations of carboxylic groups. pH variations notably impact nZVI adsorption capacity and selectivity distribution, with the highest Pb and Cd removal observed at pH 3, followed by pH 4, while the lowest removal rate occurs at pH 8.5. Pb adsorption capacity correlates with pH trends, whereas Cd exhibits slight increases up to pH 6 then tended to decrease ~~before decreasing~~ at pH 7 and 8.5. Activity of irradiated or non-irradiated nZVI on removing Cd and Pb was influenced by contact time with the contaminants.The removal effectiveness of Pb remains consistent between irradiated and non-irradiated nZVI, and improved with extended contact time up to 180 min. Conversely, non-irradiated nZVI outperforms irradiated nZVI in Cd removal, with the highest removal efficiency achieved at 180 min. Overall, both irradiated and non-irradiated nZVI demonstrate optimal performance at 180 minutes, achieving producing the highest removal efficiency.

Key words: Water pollution, Nano-zero valent Iron (nZVI) Adsorption capacity, Characterization, Affecting factors, Irradiation.

Introduction

One such development is the use of zero-valent iron nanoparticles in combination with another support material to create a nanocomposite material that functions as a point-of-use filter and a permeable reactive barrier to provide remediation capabilities. Moreover, it has been shown that utilizing direct zero-valent iron nanoparticles can eliminate a lot of pollutants from defiled water (**Kozma** et al. 2016). Then again, perilous azo colors, weighty metals, chlorinated sweet-smelling compounds, and nitro-fragrant mixtures can be generally adsorbed by zero valent iron (nZVI). As per **Huang et al**. (2018), the thin Fe_2O_3 core improves the adsorption process by surface complexation and electrostatic force. As per a recent study conducted by **Kuhn** et al. (2022), nanotechnology plays a crucial role in water treatment and remediation. It offers a wide range of benefits such as the elimination of heavy metals, deactivation of pathogens, and conversion of toxic substances into less harmful compounds. Nanomaterials act as powerful agents in purifying water, acting like superheroes. Specifically, nanoparticles effectively remove heavy metals from wastewater by adhering to their surfaces. The use of adsorbents with a large specific surface area significantly enhances their capacity to absorb heavy metals (**Liu** et al., 2020).

The researchers successfully removed heavy metals from wastewater using different nanomaterials (**Patanjali** et al., 2019). They discovered that zeolite was able to eliminate heavy metal ions, while zerovalent Nano-Fe proved effective in eliminating organic molecules containing halogens. NZVI was previously recognized as one of the most widely used and extensively studied nanomaterials during the period of heavy metal removal (**Tarekegn** et al., 2021). According to a review by **Lei et al**. in 2023, nano zero-valent iron (nZVI) has demonstrated its effectiveness as an adsorbent, reductant, and catalyst for a variety of pollutants, including organic dyes, heavy metal ions, and halogenated organic compounds It's one of the most extensively studied and utilized nanomaterials for environmental cleanup. The oxide layers of Fe

(II) and Fe (III) that structure because of the fast oxidation of metallic iron in the climate encompass the metallic iron center of the nanoparticles. The decreasing skill of metallic iron can be utilized to lessen different ecological poisons. Iron (hydr) oxide is delivered when NZVI, water, and oxygen communicate in fluid arrangements. The shell is fit for shaping synthetic mixtures and has a base thickness of 3 nm. This anodic cycle uses the center (Fe0) as an electron giver: 2e- + Fe Fe^{2+}. The outer layer of iron (hydro) oxide serves as an effective adsorbent for several contaminants, including heavy metals. In water, Fe (0) nanoparticles can exhibit different metal or ligand coordination characteristics depending on the pH of the solution. When the pH level exceeds 8, the surface of the nanoparticle undergoes a transformation, acquiring a negative charge. This enables the formation of surface complexes with metal cations. In this work, artificially combined nanocomposites zero valent iron and nano-zero valent iron were prepared. Different methods, including filtering electron microscopy (SEM), energy dispersive X-beam examination (EDX), X-beam diffraction (XRD), and Fourier change infrared spectroscopy (FTIR), were utilized to explore the exact properties of nZVI chemically synthesized for treating the wastewater polluted with Cd and Pb as representatives of weighty heavy metals (HMs).

Materials and Methods

Preparation of nZVI

Zero-valent Iron (ZVI) was prepared at nano scale using chemical methods as described below:

The production of nZVI involved the reduction of an iron salt in an aqueous solution using sodium borohydride, as described by Mokate et al. (2020). While the typical conditions for this stage of nZVI synthesis are aerobic, this experiment deviated by utilizing atmospheric conditions. The procedure commenced with the dissolution of 0.0125 M $FeCl_3$ in 50 mL of deionized water, followed by stirring at 800 rpm for ten minutes. Subsequently, 0.1 mL of ethylene glycol (EG) was introduced and stirring persisted for an additional 10 minutes. The reaction vessel was then charged with 0.0125 M $NaBH_4$, leading to the formation of ZVI as a black precipitate in an instantaneous reaction.

Polyvinylpyrrolidone + nZVI (PVP + nZVI); In this methodology, Polyethylene oxide (PEO) at a concentration of 5% (w/v) and Polyvinylpyrrolidone (PVP) at 30% (w/v) were synthesized separately by dissolving them in bi-distilled water at temperatures of 85°C and 45°C, respectively, over a duration of 40-45 minutes using a magnetic stirrer. The solutions were then combined in a ratio of 85:15 (PEO: PVP), and 0.5 g of NZVI was introduced with a magnetic stirrer until a thoroughly mixed and homogeneous solution was achieved. Subsequently, the mixture was transferred to test tubes and exposed to a 20 kGy dose of gamma radiation from a cobalt-60 source. Following the preparation and radiation steps, the hydrogels were sliced into disks and left to dry at room temperature for a period of seven days **(Thi Sinh, 2020).**

A. Characterization of Nano-zerovalent iron

FT-IR characterization

Fourier transform infrared spectroscopy (FTIR) utilizes the infrared region of the electromagnetic spectrum. In contrast to the visible range, the infrared range exhibits longer wavelengths and lower frequencies. The FTIR analysis involves a spectral resolution of 4 cm^{-1} and a scanning range from 4000 to 400 cm^{-1}. Different elements' bonds absorb infrared radiation at distinct frequencies, forming the basis for FTIR analysis. The vibrational spectra of NZVI composition were examined using a Fourier transform infrared spectrometer and a simulation instrument, specifically the NICOLET iS10, scanning the range of 4000-400 cm^{-1} with potassium bromide as the substrate. In this instance, the sample was meticulously mixed with KBr (1:10 % by mass), and the resulting substrate was compressed and ground into a disk measuring 5.0 mm in diameter and 1.0 mm in thickness. The infrared spectrum was then scanned across the 4000-400 cm^{-1} wavelength range.

An energy dispersive X-ray-equipped scanning electron microscope (SEM-EDX):

The examination of surface structures of the material of interest is conducted through scanning electron microscopy (SEM). This technique is employed to capture and analyze the surface features of the material. The Central Elemental and Isotopic Analysis Laboratory at the Atomic Energy Authority, Nuclear Research Center in Cairo, Egypt, houses a scanning electron microscope equipped with an energy dispersive X-ray spectrometer (SEM-EDX), serving as a solid surface microprobe. The SEM-EDX system has been enhanced for imaging and analyzing frozen liquid surfaces containing various solid or liquid components. With the application of low vacuum (LV) technology, the microprobe is capable of imaging and analyzing both conductors and insulators without the need for conductive coatings. The SEM model (JSM 5600 LV) was acquired from Jeol, Japan, in 1999, with the EDX component headquartered in Oxford, England.

X- ray Diffraction (XRD)

The particle sizes of tested materials determination (nm)

Nanoparticles can exhibit either an amorphous or crystalline arrangement of their constituent atoms. The degree of crystallinity is determined by the ratio of crystalline to amorphous structures. To quantify the crystallite size, the Scherrer equation comes into

play. This equation establishes a correlation between the size of sub-micrometer particles within a material and the broadening of a peak in the diffraction pattern observed in X-ray diffraction and crystallography. Named after Paul Scherrer, the Scherrer equation is a valuable tool for determining the size of powdered crystal particles. The X-ray diffraction (XRD) pattern technique contributed in assessing the particle sizes in tested materials.

The Scherrer equation can be used to determine the particle size based on the breadth of the diffraction peaks:

$$\mathbf{B\,(2\theta) = k\,\lambda\,/\,D\cdot\cos\theta}$$

$$D=\frac{0.94\times\lambda}{\beta\cos\theta}$$

Where, **D** is the average crystallite size perpendicular to the reflecting planes, **λ** is the x-ray wavelength, **θ** is the Bragg angle, β is the width of the peak in radians due to the finite size of the crystal, and the numerical constant K is a function of the crystallite shape but is generally taken as being about 1.0 for spherical particles. The shape factor has a typical value of about 0.9, but varies with the actual shape of the crystallite; but for which **Scherrer (1918)** obtained the value $2(\ln 2/\pi)^{1/2}$ =0. 93 but **Patterson, (1939)**, modified the shape factor (k) by the value = 1.107∼ 1.11.

B. Adsorption and Batch Experiments procedure

Achieving optimal performance in the adsorption process involves regulating several parameters, including contact time, temperature, pH, amount of adsorbent, and the initial concentration of the target contaminant. To create an aqueous solution containing Pb (II) and Cd (II), the requisite amounts of Pb $(NO_3)_2$ and Cd $(NO_3)_2$ were dissolved in deionized distilled water. The pH was initially adjusted within the optimal range of 3 to 8.5. Subsequently, the efficiency of removing Pb (II) and Cd (II) ions was evaluated for varying dosages of nZVI adsorbent (ranging from 0.25 to 0.75 mg). The duration of contact significantly influences the adsorption process, and kinetic experiments were conducted to determine the equilibrium time and the most fitting kinetic model. For a target pollutant concentration of 50 mg L^{-1}, the contact time was optimized within the range of 30 to 180 minutes. Equilibrium isotherm experiments were also carried out with different initial lead concentrations (ranging from 10 to 100 mg L^{-1}) to examine the impact on adsorption efficiency. The adsorption process is intricately linked with contact time, and kinetic studies were performed to identify the optimal kinetic model and equilibrium period. Exposure times between 30 and 180 minutes were found to be ideal for target pollutants with a concentration of 50 mg L^{-1}. Additionally, equilibrium isotherm experiments explored the effect of initial lead concentration on adsorption efficiency, covering a range from 10 to 100 mg L^{-1}.

In these studies, the initial adsorption temperature was maintained at 25°C, while the initial pH of the solutions was set at 6 and 25, respectively. The research also delved into the impact of temperature, specifically within the range of 25 to 45°C, on the removal efficiency of Pb (II). Batch studies were carried out using a 100 ml polyethylene bottle, incorporating 0.5 g of sorbent and 50 ml of Pb and Cd solution, all adjusted to the appropriate pH and concentration. The mixture was stirred using a shaker set to 200 rpm to ensure thorough mixing and representative results. For each batch adsorption experiment, three replicates were prepared for every and concentration of aqueous solutions. During the adsorption trials, multiple samples were collected, filtered through Whatman filter paper no. 42, and the concentration of the target pollutant was determined in the supernatant immediately after filtration using Inductively Coupled Plasma (ICP).

The adsorption capacity of the adsorbent qe (mg g^{-1}) and the removal efficiency of Pb (II) and Cd (II) (R %) were calculated using equations (1) and (2).

$$R\,\% = \frac{(Co-Ce)}{Co}\times 100 \qquad (1)$$

The adsorption capacity was calculated using the following equation 2;

$$Qe\ (mg/g) = \frac{(Co-Ce)}{M}\times V \qquad (2)$$

The distribution coefficient (Kd) or selectivity distribution were determined through the following Equation (3).

$$K_d = \frac{\text{Amount of metal ion adsorbed onto sorbent}}{\text{Amount of metal ion remaining in the solution}} \times \frac{V}{M} = \frac{(Co-Ce)}{(Ce)} \times \frac{V}{M} \qquad (3)$$

Where, Co is the initial concertation and Ce is the equilibrium concentration in mg/L. Qe is amount adsorbed at equilibrium in mg/g, V is the volume of the solution in liters, and M is the weight of the adsorbent in grams.

Statistical Data analysis

Microsoft Excel was used for statistical analysis in order to calculate the variance, mean, and standard deviation. The adsorption capacity of the tested materials was estimated using the adsorption isotherms. The adsorption mechanism and its potential in the rate control step were investigated using kinetic models.

Results and Discussion

nZVI characterization by EDX.

The EDX analysis, which demonstrated the types of adsorbent materials both before and after gamma-ray irradiation at a dose of 20 kGy, as well as the existence of the predicted elements in the structure, approved the assessment of nZVI's chemical composition (Table 1). Elements O, Na, Al, Si, S, Cl, and Fe are present in nZVI, as Fig. 1 illustrates.

Table 1. EDX of anticipated elements composition (%) in irradiated and non-irradiated nZVI, exposed to 20 kGy of gamma ray.

Irradiation	Elements							Total
	O	Na	Al	Si	S	Cl	Fe	
Non-irradiated	17.07	0.07	0.04	0.10	0.50	1.02	81.21	100
Irradiated	15.28	0.09	0.09	0.22	0.73	0.52	83.07	100

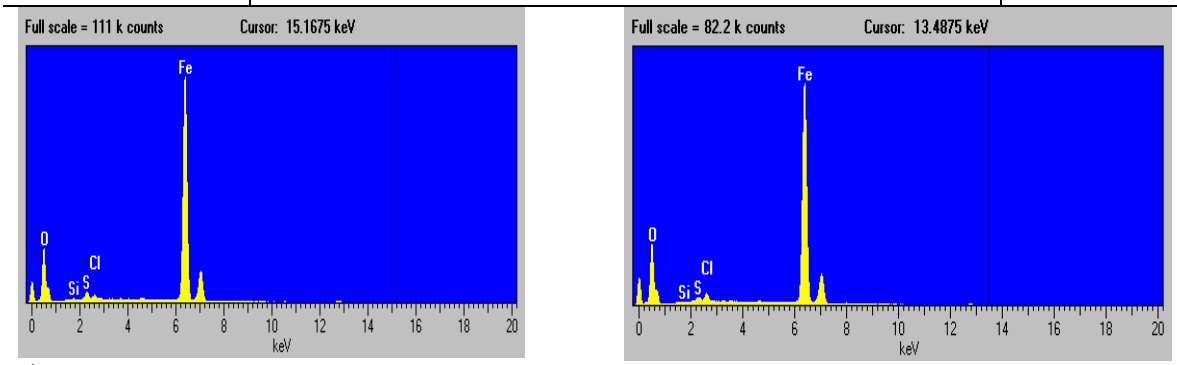

a) **b)**

Fig.1: EDX of anticipated elements in NZVI **a**) non-irradiated and **b**) irradiated with gamma ray at dose 20 kGy.

Characterizing the nano crystallite size (D) by X-ray diffraction (XRD).

In 1918, the Scherrer Equation was created to determine the nano crystallite size (D) using XRD radiation with a wavelength of λ (nm). This was achieved by measuring the whole width at half maximum of peaks (β) in radians, which could be found at any 2θ in the pattern.

$$B = \frac{K\lambda}{D \cos\theta}$$

If crystals are smaller than 1000 Å or 100 nm, the Scherrer equation estimates the thickness of the crystallites. The most straightforward method to derive the Scherrer equation is to use Bragg's Law's derivation, which is $\lambda = 2 \sin d\theta$.

$$D = \left(\frac{0.94\,\lambda}{B \cos\theta}\right)$$

Where, λ=0.154 nm is the wavelength of the X-rays, (β) is the diffraction peak (β2θ) (expressed in radians) is the full width at the half maximum (FWHM) of the diffraction peak or integral breadth and θ is the Bragg angle and K (the Scherrer constant) is shape factor which varies with the type of crystal structure. The constant of proportionality, K depends on ~~the~~ how the width is determined, the shape of the crystal, and the size distribution. The most common values for K are: 0.94 for FWHM of spherical crystals with cubic symmetry.

The XRD pattern indicates that the nZVI in its composition is crystallite size 60.80 nm. The result of crystal size had shown cubic structure (Table 2).

Table 2: XRD pattern used for determination of the nano crystallite size of nZVI.

Tested Materials	D	I/Io	2θ	θ deg	θ Rad	β FWHM (deg)	*β Rad*	Crystallite size (nm)
NZVI	**3.0988**	**100**	**28.7875**	**14.3938**	**0.2512**	**0.1355**	**0.002356**	**60.8009**

nZVI Characterization by SEM

The surface morphology of synthesized nZVI as seen by SEM is shown by Fig. (2). This figure revealed that the sample's surface porosity and texture were better developed. This vividly illustrates how a porous surface forms and its uniformly dispersed globular shape. These globular structures could therefore be to blame for the increase in surface area and pores that are needed for an efficient adsorbent for Pb^{+2} and Cd^{+2}. ZVI showed up as cubic crystals with 60.80 nm crystallite sizes.

a) Non-irradiated **b)** Irradiated

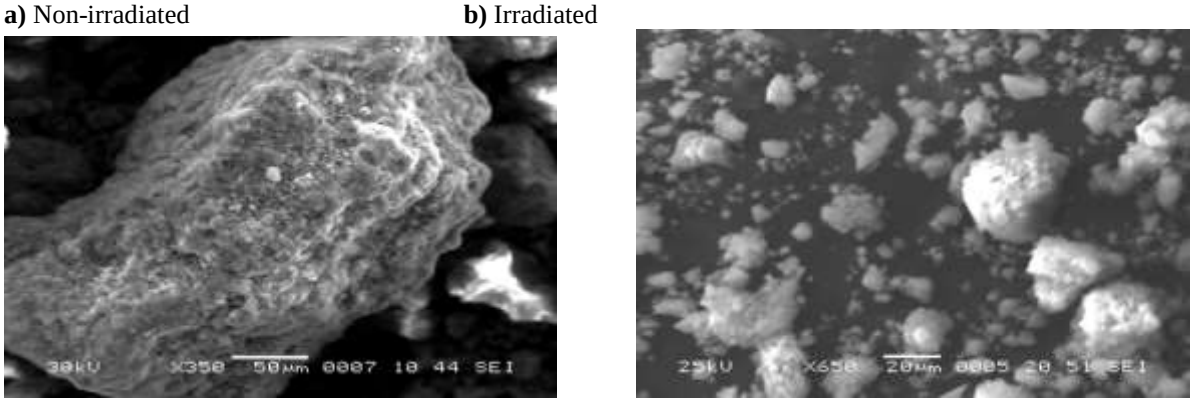

Fig. 2: SEM micrographs images of nanozero-valent iron, a) non-irradiated and b) irradiated by gamma ray at dose 20 kGy.

nZVI characterization by FT-IR spectroscopy

After the procedure, the FTIR spectra of nZVI (control) and nZVI bind with Pb^{2+} or Cd^{2+} were obtained and illustrated by Figs. (3 - 6) and were in the 400–4000 cm^{-1} range. Furthermore, Fe-O stretching vibration is correlated with absorption peaks seen at 447 and 682 cm^{-1}.

As can be seen in the above-mentioned Figures, the O-H stretching vibration of carboxylic groups is responsible for the absorption peak at 3420 cm^{-1} which shifted to 3428 and 3430 cm^{-1} and at the detectable peaks observed at wavenumbers 3847 attributed to OH^- stretching before and after irradiation when loading with Pb and Cd. A moiety is typically used to denote a portion of a molecule; for example, the alcohol moiety in an ester R_1COOR_2 is R_2O. The band that occurred at these bands as well as at 1637 cm^{-1} is attributed to the O-H stretching and bending vibration band of the water moiety adsorbed on the nZVI surface. A little piece of a molecule shouldn't be referred to by this phrase **(IUPAC, 1997)**. According to **Li, *et al.* (2022)**, this indicates that a ferric oxyhydroxide (FeOOH) layer has formed on NZVI. Following Pb^{2+} or Cd^{2+} adsorption, the peaks at 1302 and 1100 cm^{-1} were displaced, indicating the loss of water molecules **(*Adil et al.*, 2023)**. Fe-O-Pb adsorption with bending modes at 740 and 689 cm^{-1} was suggested by the shift in FT-IR intensity between 1080 and 872 cm^{-1}. According to ***Adil et al.* (2023)**, the IR peak intensity falls around 1000 cm^{-1}, indicating that lead adsorption has broken a hydrogen bond. Additionally, a number of oxygen functional groups visible in the recently produced nZVI's FTIR spectrum could serve as readily accessible adsorption sites. The oxygen atoms in the -OH and C-O groups can supply free electrons to interfere with the vacant orbitals of contaminating ions. **Yang *et al.* (2018)** noted that the marginal shifting of peaks in the 1626–1020 cm^{-1} region further suggests the efficient desorption of Fe_2/Fe_3 ions on the surface of nZVI through chelating with oxygen-containing groups.

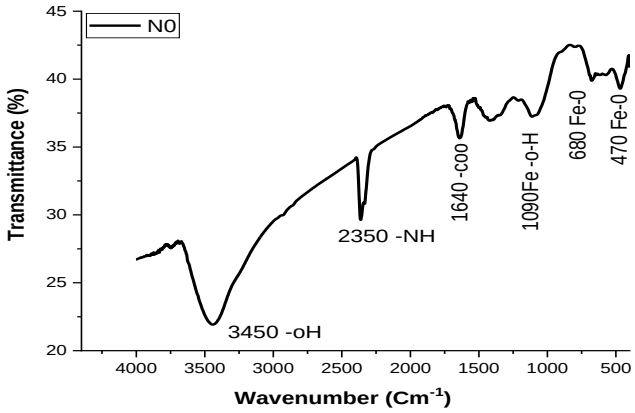

Fig. 3: FT-IR spectra of nZVI as an adsorbent material without any treatments.

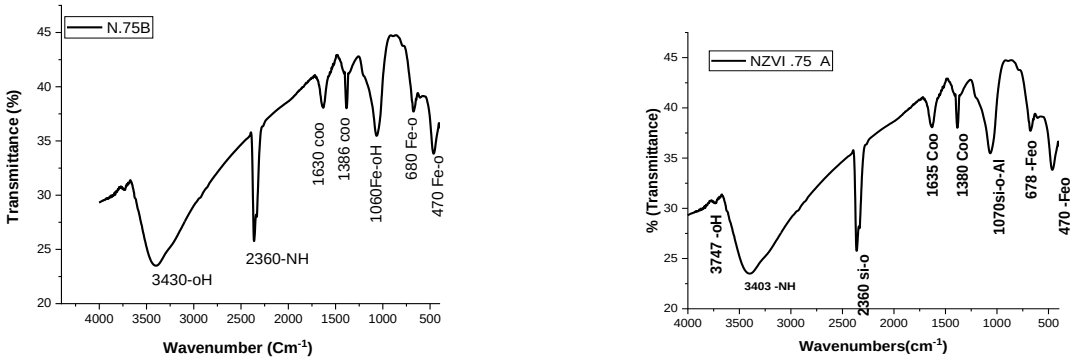

Fig. 4: FT-IR spectra of nZVI as adsorbent material at dose rate 0.75 (g), **a)** non-irradiated and **b)** irradiated with gamma ray at dose 20 kGy.

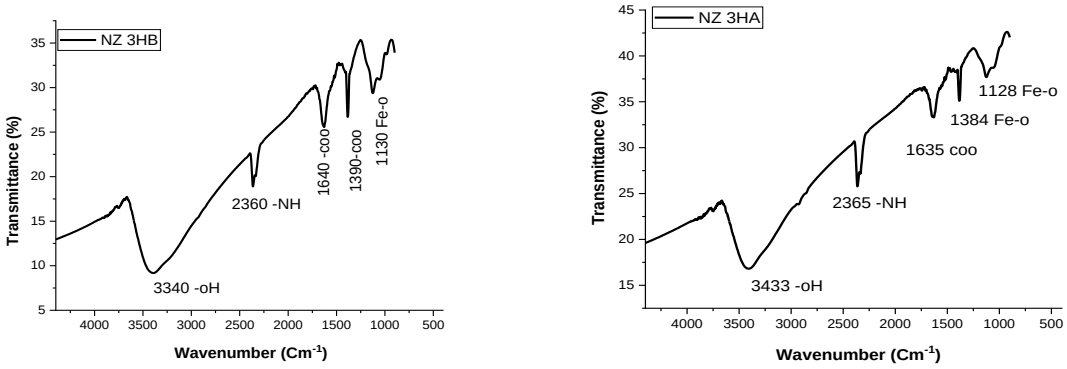

Fig. 5: FTIR spectra of nZVI as adsorbent material after 3h contact time, **a)** non-irradiated and **b)** irradiated with gamma ray at dose 20 kGy.

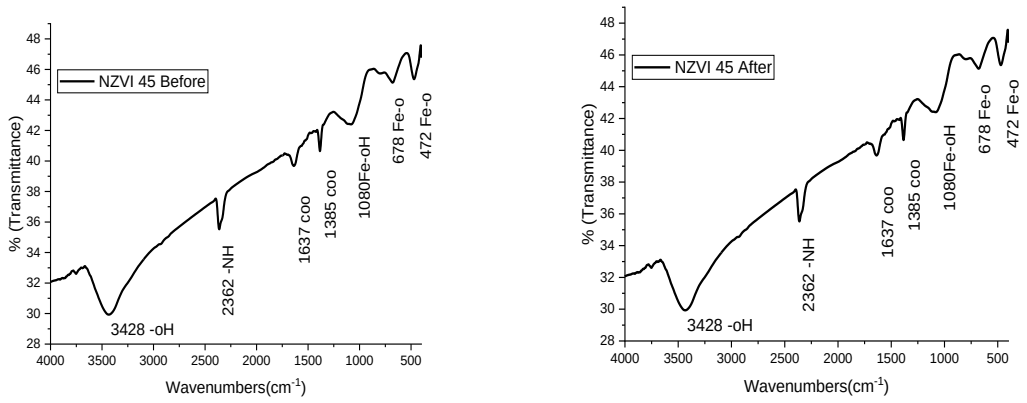

Fig. 6: FT-IR spectra of nZVI as adsorbent material after exposed to 45 °C temp., **a)** non-irradiated and **b)** irradiated with gamma ray at dose 20 kGy.

Impact of nZVI on Cd and Pb adsorption

Effect of pH and contact time

Removal of Cd and Pd from the contaminated wastewater was examined under different pH and dose rates of adsorbent (nZVI). In this respect, adsorption of these contaminants on nZVI as removal percent, adsorption capacity and selectivity distribution were frequently affected by gradual increases in pH (Table 3). Generally, all these measurements tended to decrease with increasing solution pH. The maximum removal was detected at pH 3 followed by those at pH 4 while the lowest removal percent was indicated at pH 8.5. Similar trend was noticed with adsorption capacity of Pb, while Cd showed slight increases with increasing pH up to 6 then tended to decrease with pH 7 and 8.5. In addition, selectivity distribution was severely decreased with increasing pH values recording the lowest Pb at pH 8.5 which relatively accounted for 6.3% from those recorded at pH 3. On the other hand, in case of Cd, selectivity distribution was increased due to pH increments.

Table 3. Effect of pH on Pb^{+2} and Cd^{+2} Removal, Adsorption Capacity and Kd (selectivity distribution) using nZVI nanomaterials.

Measurements	Element	pH				
		3	5	6	7	8.5
Removal%	Pb	95.22	89.32	81.35	60.57	55.71
	Cd	80.18	89.51	83.21	75.70	53.63
Adsorption Capacity (mg g^{-1})	Pb	4.68	4.39	4.00	2.97	2.74
	Cd	3.91	4.36	4.06	3.69	2.61
Kd (selectivity distribution)	Pb	1996.12	836.41	436.39	153.63	125.80
	Cd	404.52	853.41	495.51	311.52	115.68

Concerning the effect of contact time on adsorption of Pb and Cd, data illustrated by Fig. 7, reflected that removal efficiency of Pb by either irradiated or non-irradiated nZVI was nearly closed to each other but still improved with increasing contact time up to three hours (180 min). Cd removed by non-irradiated nZVI was significantly higher than those removed by irradiated one. Both irradiated and non-irradiated n ZVI resulted in the highest RE % at 180 min contact time. These results are, to some extent, in the same direction with previous research of others. In this way, When **Song *et al.* (2023)** looked at nZVI that had been synthesized and connected to coffee grounds, they discovered that the highest adsorption capacity from the Langmuir model was 814.95 mg/g for Pb^{2+} and 196.06 mg/g for Cd^{2+}, respectively, under adsorption isotherms at pH 6 and 20°C. Since the removal of Pb^{2+} involves reduction, the adsorption isotherm did not fit the experiment's data very well. For Pb^{2+} and Cd^{2+}, it took one hour and eight hours, respectively, to attain equilibrium. The dynamics of heavy metal adsorption are effectively explained by the pseudo-2nd order kinetic model, indicating that chemisorption is most likely the process. Eighty percent of Pb^{2+} and sixty percent of Cd^{2+} were rapidly carried by surface diffusion, whereas residuals were transported by interparticle diffusion, according to the mass transfer mechanism investigation. Recently, **Park *et al.* (2019)** found that the removal effectiveness rose with pH increases from 2 to 4 and was at its highest at pH 4 for both Pb (II) and Cd (II) adsorption. The optimal pH range was found to be between 4 and 6. nZVI is thought to be a viable adsorbent for the removal of heavy metals because it has extensive active sites and functional groups **(Zou *et al.*, 2016; Hasan *et al.*, 2020)**. Accordingly, it was discovered that nZVI-based nanoparticles exhibit strong and selective Cd^{2+} adsorption, with a maximum Cd^{2+} adsorption capacity of 290 mg/g following a 5-hour reaction period at 25°C **(Xu *et al.*, 2023)**. Moreover, the surface of nZVI may create iron hydroxides or oxides, which could improve the adsorption process in a Fe0-HO system **(Zhu *et al.*, 2017)**. Additionally, it is thought that adsorption employing materials based on iron is non-toxic and economical **(Alazaiza *et al.*, 2022). Abukhadra *et al.* (2018)** found that the maximum adsorption capacity for Zn^{2+}, Co^{2+}, and Cu^{2+} was 149.25, 106.4, and 147.5 mg/g, respectively, using materials based on nZVI. The limit was achieved after 240 minutes for Zn^{2+}, Co^{2+}, and 120 minutes for Cu^{2+}. The adsorption isotherm was fitted with the Langmuir model.

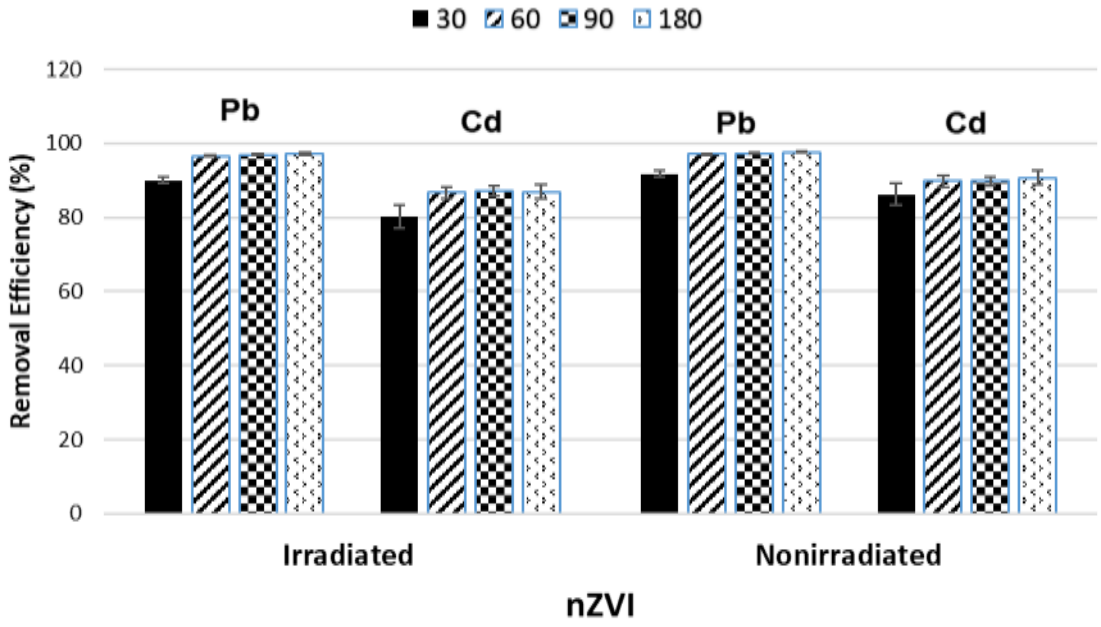

Figure 7. Effects of contact times (minutes) on the removal efficiency (%) of Cd and Pb in artificial contaminated wastewater using irradiated and nonirradiated nZVI absorbant.

Many researchers have generally linked the precipitation (the creation of insoluble minerals) of heavy metals to electrostatic interactions, surface complexation between hydroxyl and carboxyl groups, and positively charged metal ions **(Li *et al.*, 2018; Yang *et al.*, 2020; Sharma *et al.*, 2018).** conducted a review of numerous studies that demonstrated the exceptional adsorption ability of nanocomposites for heavy metals (HMs), as well as the greater simultaneous adsorption rates of HMs compared to bulk materials. These investigations generally addressed factors like beginning concentration, contact time, and adsorbent dosage, and they verified that the simultaneous removal rate of heavy metals (HMs) declined as pH increased. **Sepehri *et al.* (2023)** expounded on their findings, indicating that lead absorption can be inhibited at pH values higher than 6 due to the formation of several hydroxyl low-soluble species, including Pb (OH). Simultaneously, when the pH increased, Fe (II) and Fe (III) precipitates slowly developed, covering the nZVFe particle shell. This decreased the nanocomposite's ability to adsorb substances, as reported by Pei and Liu in 2022. **Sepehri *et al.* (2023)** determined that 700 minutes was the maximum duration for Pb (II) adsorption on nZVFe–RSAC (rice straw activated carbon) with regard to the contact time effect.

Conclusion

The use of different characterization tools has highlighted that nZVI in its composition is a 60.8 nm crystalline and dispersed spherical structure as well as porous surface formation.

The observable peaks detected at wavenumber 3847 are attributable to OH^- stretching before and after irradiation during Pb and Cd loading. The absorption peak at 3420 cm^{-1} shifts to 3428 and 3430 cm^{-1} due to the O-H stretching vibration of the carboxylic groups.

The removal rate, adsorption capacity, and selectivity distribution were severely affected with increasing pH units.

These parameters were frequently affected by time contact with Cd and Pb in solution but improved with increasing contact time up to 180 min. In this regard, irradiation had no detectable effect on Pb and Cd adsorption with the values obtained for irradiated and unirradiated nZVI being almost close to each other. On the other hand, characterization and batch tests showed how useful nZVI material is as an absorbent for removing Pb and Cd out of contaminated solutions.

References

Abukhadra M.R.; Dardir F. M;, Shaban M., Ahmed E.A.and Soliman M.F. (2018). Superior removal of Co^{2+}, Cu^{2+} and Zn^{2+} contaminants from water utilizing spongy Ni/Fe carbonate-fluorapatite; preparation, application

and mechanism, Ecotoxicol. Environ. Saf., 157, 358-368.

Adil, M., Giri, B. R., Mai, T. V. T., Huynh, L. K., and Farooq, A. (2023). High-temperature mid-IR absorption spectra and reaction kinetics of 1, 3-dioxolane. *Proceedings of the Combustion Institute*, *39*(1), 621-631.

Alazaiza M.Y.D., Albahnasawi A., Copty N.K., Bashir M.J.K., Nassani D.E., Al Maskari T., Abu Amr S.S.and Abujazar M.S.S. (2022). Nanoscale zero-valent iron application for the treatment of soil, wastewater and groundwater contaminated with heavy metals: a review. *Desalination and Water Treatment* 253, 194–210 doi: 10.5004/dwt.2022.28302

Huang X.Y., Ling L. and Zhang W.X. (2018). Nanoencapsulation of hexavalent chromium with nanoscale zero-valent iron: high resolution chemical mapping of the passivation layer. J Environ Sci 67:4-13

IUPAC. Compendium of Chemical Terminology, 2nd ed. (the "Gold Book"). Compiled by A. D. McNaught and A. Wilkinson. Blackwell Scientific Publications, Oxford (1997). Online version (2019-) created by S. J. Chalk. ISBN 0-9678550-9-8. https://doi.org/10.1351/goldbook.

Kozma, G., Rónavári, A., Kónya, Z., and Kukovecz, A. (2016). Environmentally benign synthesis methods of zero-valent iron nanoparticles. *ACS Sustainable Chemistry & Engineering*, *4*(1), 291-297.

Kuhn, R., Bryant, I. M., Jensch, R., and Böllmann, J. (2022). Applications of environmental nanotechnologies in remediation, wastewater treatment, drinking water treatment, and agriculture. *Applied Nano*, *3*(1), 54-90.

Lei, Z., Song, X., Ma, G., Zhao, T., Meng, K., Zhang, M., ... and Dai, L. (2023). A review of recent studies on nano zero-valent iron activated persulfate advanced oxidation technology for the degradation of organic pollutants. *New Journal of Chemistry*.

Li Z., Wang L., Meng J., Liu X., Xu J.and Wang F. (2018). Zeolitesupported nanoscale zero-valent iron: New findings on simultaneous adsorption of Cd (II), Pb (II), and As (III) in aqueous solution and soil. J Hazard Mater; 344:1-11. doi:10.1016/j.jhazmat.2017.09.036.

Li, Y., Li, S., Hu, B., Zhao, X., and Guo, P. (2022). FeOOH and nZVI combined with superconducting high gradient magnetic separation for the remediation of high-arsenic metallurgical wastewater. *Separation and Purification Technology*, *285*, 120372.

Park M.H., Jeong S., Lee G., Park H. and Kim J.Y. (2019). Removal of aqueous-phase Pb(II), Cd(II), As(III), and As(V) by nanoscale zero-valent iron supported on exhausted coffee grounds. Waste Management 92, 49-58.

Patanjali P., Singh R. and Kumar A. (2019). Nanotechnology for water treatment: a green approach. In: Iravani S (ed) Shukla AK. Green Synthesis, Characterization and Applications of Nanoparticles, pp 485-512

Ren, J.; Zheng, L.; Su, Y.; Meng, P.; Zhou, Q.; Zeng, H.; Zhang, T. and Yu, H. (2022). Competitive adsorption of Cd (II), Pb (II) and Cu (II) ions from acid mine drainage with zero-valent iron/phosphoric titanium dioxide: XPS qualitative analyses and DFT quantitative calculations. Chem. Eng. J., 445, 136778.

Scherrer P (1918) Estimation of the size and internal structure of colloidal particles by means of röntgen. Nachr Ges Wiss Göttingen 2:96–100

Sepehri, S.; Kanani, E.; Abdoli, S.; Rajput, V.D.; Minkina, T. and Asgari Lajayer, B. (2023). Pb(II) Removal from Aqueous Solutions by Adsorption on Stabilized Zero-Valent Iron Nanoparticles-A Green Approach. Water, 15, 222. https://doi.org/10.3390/w15020222

Sharma R., Raghav S., Nair M. and Kumar D. (2018). Kinetics and adsorption studies of mercury and lead by ceria nanoparticles entrapped in tamarind powder. ACS Omega; 3(11):14606-19. doi: 10.1021/acsomega.8b01874.

Song, H., Liang, W., Luo, K., Wang, G., Li, Q., Ji, X., and Peng, C. (2023). Simultaneous stabilization of Pb, Cd, and As in soil by rhamnolipid coated sulfidated nano zero-valent iron: Effects and mechanisms. *Journal of Hazardous Materials*, *443*, 130259.

Tarekegn, M. M., Hiruy, A. M., and Dekebo, A. H. (2021). Nano zero valent iron (nZVI) particles for the removal of heavy metals (Cd 2+, Cu 2+ and Pb 2+) from aqueous solutions. *RSC advances*, *11*(30), 18539-18551.

Thi Sinh (2020): Heavy metal removal applications using adsorptive membranes, Nano Convergence, (2020), 7:36.

Xu, Y., Cao, S., Chen, X., Li, J., Liu, H., Gao, Y., Wen, S., Guo, J., Shi, X. and Xue, W., 2023. Enhanced immobilization of cadmium in contaminated paddy soil by biochar-supported sulfidized nanoscale zero-valent iron. *Journal of Soils and Sediments*, pp.1-16.

Yang D., Wang L., Li Z., Tang X., He and M., Yang S. (2020). Simultaneous adsorption of Cd (II) and As (III) by a novel biochar-supported nanoscale zero-valent iron in aqueous systems. Sci Total Environ; 708:134823. doi: 10.1016/j. scitotenv.2019.134823.

Yang F, Zhang S, Sun Y, Cheng K, Li J and Tsang D C W 2018 Fabrication and characterization of hydrophilic corn stalk biochar-supported nanoscale zero-valent iron

composites for efficient metal removal. Bioresour. Technol. 265 490.

Zhu S., Ho S.H., Huang X., Wang D., Yang F., Wang L., Wang C., Cao X. and Ma F. (2017). Magnetic nanoscale zero-valent iron assisted biochar: interfacial chemical behaviors and heavy metals remediation performance, ACS Sustainable Chem. Eng., 5, 9673-9682.

Zou Y., Wang X., Khan A., Wang P., Liu Y., Alsaedi A., Hayat T., and Wang X. **(2016).** Environmental remediation and application of nanoscale zero-valent iron and its composites for the removal of heavy metal ions: a review, Environ. Sci. Technol., 50 7290-7304.

توصيف الحديد النانوي صفرى التكافؤ المخلق كيميائياً (nZVI) والمُعد لإزالة الملوثات من المياه الملوثة

[2]ابراهيم عبد النبى ابراهيم شهاب . [1]أ.د/ هيثم محمد شحاته سالم ,[2]أ.د / سليمان محمد سليمان , [2]أ.د / يحيى جلال محمد جلال و[1]أ.د / محمد على عبد السلام

[1]قسم الأراضى، والمياه كلية الزراعة، مشتهر، جامعة بنها.

[2] قسم بحوث الأراضى والمياه،مركز البحوث النووية ،هيئة الطاقة الذرية أبوزعبل 13759 –مصر

يعتبر تلوث المياه قضية عالمية. نظرًا لزيادة الطلب على المياه العذبة، تم إيلاء المزيد من الاهتمام لإزالة الملوثات الطبيعية أو البشرية الناشئة فى المياه والتي أصبحت أكثر تعقيدًا وصعوبة. لذلك، يهدف هذا العمل إلى تحضير وتوصيف مادة نانوية تم تصنيعهما كيميائيًا مثل حديد صفر التكافؤ النانوي (nZVI) لاستخدامهما كمواد ماصة لملوثات العناصر الثقيلة الموجودة في الماء. أثبت توصيف nZVI وجود العناصر المتوقعة في بنية المواد الممتزة المشعة أو غير المشعة. إن nZVI في تركيبته هو حجم بلوري 60.80 نانومتر ويظهر على شكل بلوري مكعب وهو ما يشير إليه SEM. أوضح فحص FTIR أن اهتزاز التمدد O–H للمجموعات الكربوكسيلية هو المسؤول عن ذروة امتصاص Pb وCd. تأثرت قدرة الامتزاز nZVI والتوزيع الانتقائي في كثير من الأحيان بالزيادات التدريجية في الرقم الهيدروجيني. تم الكشف عن الحد الأقصى لإزالة الرصاص والكادميوم عند الرقم الهيدروجيني 3 تليها تلك عند الرقم الهيدروجيني 4 بينما تمت الإشارة إلى أقل نسبة إزالة عند الرقم الهيدروجيني 8.5. ولوحظ اتجاه مماثل مع قدرة امتصاص الرصاص، بينما أظهر الكادميوم زيادات طفيفة مع زيادة الرقم الهيدروجيني حتى 6 ثم يميل إلى الانخفاض مع الرقم الهيدروجيني 7 و 8.5. وجد أن نشاط nZVI المشعع أو غير المشعع يتأثر بوقت التلامس مع المادة الملوثة في المحلول. في هذا الصدد، كانت كفاءة إزالة Pb إما بواسطة nZVI المشعع أو غير المشعع قريبة تقريبًا من بعضها البعض ولكنها لا تزال تتحسن مع زيادة وقت الاتصال حتى 180 دقيقة. كان Cd الذي تمت إزالته بواسطة nZVI غير المشعع أعلى بكثير من تلك التي تمت إزالتها بواسطة nZVI المشعع. أدى كل من n ZVI المشعع وغير المشعع إلى أعلى نسبة إزالة في وقت التلامس لمدة 180 دقيقة.